NJC

Cite this: *New J. Chem.*, 2011, **35**, 2557–2563

www.rsc.org/njc

PAPER

Effect of main ligands on organic photovoltaic performance of Ir(III) complexes†

Woochul Lee,‡[a] Tae-Hyuk Kwon,‡[ab] Jongchul Kwon,[a] Ji-young Kim,[c] Changhee Lee[c] and Jong-In Hong*[a]

Received (in Montpellier, France) 27th May 2011, Accepted 26th July 2011
DOI: 10.1039/c1nj20446g

The photovoltaic performance of devices fabricated using three iridium complexes (**1**, **2**, and **3**) containing different main ligands (1-phenylisoquinoline, (4-isoquinolin-1-yl-phenyl)diphenylamine, and 1-pyren-1-yl-isoquinoline for **1**, **2**, and **3**, respectively) was investigated. Two different devices, one fabricated by spin coating and one produced by vacuum deposition, were tested. Among the bulk heterojunction solar cells (BHJCs) fabricated by spin coating, the cell fabricated using **2** had the highest power conversion efficiency (PCE, 0.50%). The PCEs of **1** and **3** were 0.43% and 0.34%, respectively. These results suggested that the superior hole-transport ability of the triphenylamine moiety in **2** was responsible for the high photovoltaic performance of the device fabricated using this complex. This assumption was confirmed by fabricating electron-only devices using the three Ir complexes and comparing the turn-on voltage of each device. The photovoltaic performance of device C fabricated by the vacuum co-deposition of **2** and C_{60} in a 50 nm-thick active layer was 50% higher than that of device A (bilayer heterojunction solar cell) and device B (fabricated by the co-deposition of **2** and C_{60} with a 30 nm-thick active layer).

Introduction

Recently, the energy crisis and environmental problems have led to intensification of the search for alternative energy sources. Photovoltaic cells are considered a viable solution to these problems. Specifically, organic photovoltaic devices (OPV) are a promising alternative to silicon solar cells owing to their flexibility, high absorption coefficient, ease of fabrication, and most importantly, low manufacturing cost. In addition, the chemical structure of the donor materials can easily be modified to achieve the desired electronic properties. Organic heterojunction solar cells (OHSCs) comprise separate donor and acceptor layers analogous to a classical p–n junction.[1–5] In such bilayer cells, dissociation of photogenerated excitons occurs at the interface between the donor (D) and the acceptor (A). Hence, the power conversion efficiency is limited by the average exciton diffusion length, which in turn determines the maximum thickness of the active layers.[6] Bulk heterojunction solar cells (BHJCs)[7–10] have been proposed as a possible solution to this problem. In these devices, the acceptor molecules are uniformly distributed in the donor matrix resulting in a three-dimensional network of photoinduced charge-generating interfaces. An efficiency of more than 7% was recently achieved using a BHJC composed of a benzodithiophene polymer derivative (PTB7) and PCBM.[10] However, efficient BHJCs are relatively difficult to fabricate because of the difficulty involved in controlling the morphology of their active layer. Further, it is necessary to use high-purity materials to obtain BHJCs with long-term stability and high efficiency. One of the primary reasons for the low efficiency of OHSCs is the short (exciton) diffusion length of the donor material. Therefore, it is essential to develop organic dyes composed of donor molecules with long exciton diffusion lengths to obtain high PCE.

In general, the conversion of solar energy to electrical energy involves four major steps: absorption of light and generation of excitons, diffusion of excitons, dissociation of excitons, and charge accumulation at the electrodes.[9] To achieve high PCE, it is necessary to synthesize organic materials that can absorb near-infrared (NIR) radiation, because approximately 50% of the total solar photon flux is in the NIR region.[4] Moreover, the organic active layer must be sufficiently thick to ensure strong light absorption. However, the exciton diffusion length (5–10 nm) of singlet materials limits the absorption depth required for efficient light absorption.[11b] Thus, synthesis of donor materials that have a long exciton

[a] *Department of Chemistry, College of Natural Sciences, Seoul National University, Seoul, 151-747, Korea. E-mail: jihong@snu.ac.kr; Fax: +82-2-889-1568; Tel: +82-2-880-6682*
[b] *School of Chemistry, Bio21 Institute, University of Melbourne, Parkville, Victoria 3010, Australia*
[c] *School of Electrical Engineering and Computer Science, Inter-University Semiconductor Research Center, Seoul National University, Seoul 151-742, Korea. E-mail: chlee7@snu.ac.kr*

† Electronic supplementary information (ESI) available: Cyclic voltammograms and data of an electron-only OLED device. See DOI: 10.1039/c1nj20446g

‡ These authors contributed equally to this study.

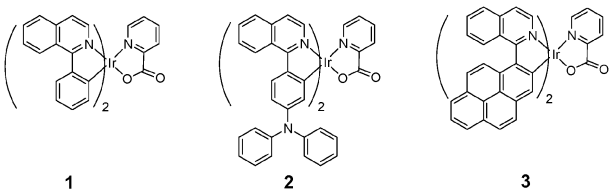

Scheme 1 Molecular structures of iridium complexes **1–3**.

diffusion length is essential for the production of efficient active layers. The exciton diffusion length depends on the charge mobility and lifetime of the donor. Accordingly, organic triplet materials, which have relatively long lifetimes, are expected to be suitable alternatives to singlet materials.[5,11]

Iridium (Ir) complexes are increasingly being used in organic light emitting Diodes (OLEDs) because the strong spin–orbit coupling in Ir allows efficient intersystem crossing (ISC) between the singlet and triplet excited states; thus, an internal quantum efficiency of 100% can be achieved.[12] Moreover, owing to the relatively long-lived excited state formed in metal-to-ligand charge-transfer (MLCT) processes, the excitons formed in Ir complexes may have a long lifetime, which favors the subsequent exciton dissociation. However, in organic solar cell research, very few studies have focused on the use of Ir complexes for active layer formation, even though organic triplet materials are suitable for the aforementioned purpose.[5,11]

In this study, the photovoltaic properties of Ir complexes with isoquinoline-based ligands were investigated. As shown in Scheme 1, to increase the power conversion efficiency of the standard Ir complex, we made two simple changes to the parent structure **1**: (1) addition of a triphenylamine unit at the 2 position of the isoquinoline moiety of **2**, and (2) addition of a pyrene unit to the isoquinoline unit to increase the absorption range. Triphenylamine is known to be a good hole-injecting/transporting material for OLEDs.[13,14] Devices were fabricated by spin coating using complexes **1–3** and their efficiencies were then compared with that of a bilayer device fabricated from **2** by vacuum deposition.

Experimental section

Materials and instruments

All organic chemicals were purchased from Aldrich and TCI. Iridium(III) chloride trihydrate was obtained from Strem. Solar cell materials including CuPc, fullerene, PCBM, and 2,9-dimethyl-4,7-diphenyl-1,10-phenanthroline (BCP) were purchased from Luminescence Technology Corporation (Taiwan). Poly(styrene sulfonic acid)-doped poly(ethylenedioxythiophene) (PEDOT:PSS, Baytron VP Al 4083) was purchased from Bayer. Analytical thin-layer chromatography was conducted using Kieselgel 60F-254 plates purchased from Merck. Column chromatography was conducted using a Merck silica gel 60 (70–230 mesh) column. All solvents and reagents used in this study were commercially available and used without further purification unless otherwise specified. ^{1}H and ^{13}C NMR spectra were recorded using an Advance 300 or 500 MHz Bruker spectrometer. UV-vis spectra were recorded using a Beckman DU 650 spectrophotometer. Mass spectra were obtained using a gas chromatograph-mass spectrometer (JEOL, JMS-AX505WA, HP 5890 Series II). Fluorescence spectra were recorded with a Jasco FP-7500 spectrophotometer. The CV measurements were made in a 0.1 M Bu_4NPF_6/acetonitrile solution using a CH Instruments 660 electrochemical analyzer (CH Instruments, Inc., Texas). The Ag reference electrode was calibrated using a ferrocene/ferrocenium redox couple. The performance of the device was measured under AM 1.5 illumination (100 mW cm^{-2}) using a solar simulator (Newport, 91160A) and Solar Cell IPCE Measurement System (McScience, K3100). The light intensity at each wavelength was calibrated using the standard Si solar cell as a reference. OLED performances were obtained using a PR 650 spectroradiometer and a source meter (Keithly 2400) connected to a computer was used to operate the device.

Synthesis

The main ligands in complexes **1–3** were synthesized according to previously described methods, with some modifications (Scheme 2).[15] Cyclometalated Ir-μ-chloro-bridged dimers (general formula: $C\hat{}N_2Ir(\mu\text{-}Cl)_2IrC\hat{}N_2$) were synthesized using a modified version of the method proposed by Nonoyama[16] and then coupled with picolinic acid in 2-ethoxyethanol to produce complexes **1**, **2**, and **3**.

$IrCl_3{\cdot}nH_2O$ was mixed with 2–2.5 equiv. of a cyclometalating ligand in a 3 : 1 mixture of 2-methoxyethanol and water, after which the mixture was refluxed for 6–7 h. The reaction mixture was then cooled to room temperature, after which more water was added to precipitate the product. The resulting mixture was subsequently filtered through a Büchner funnel and then

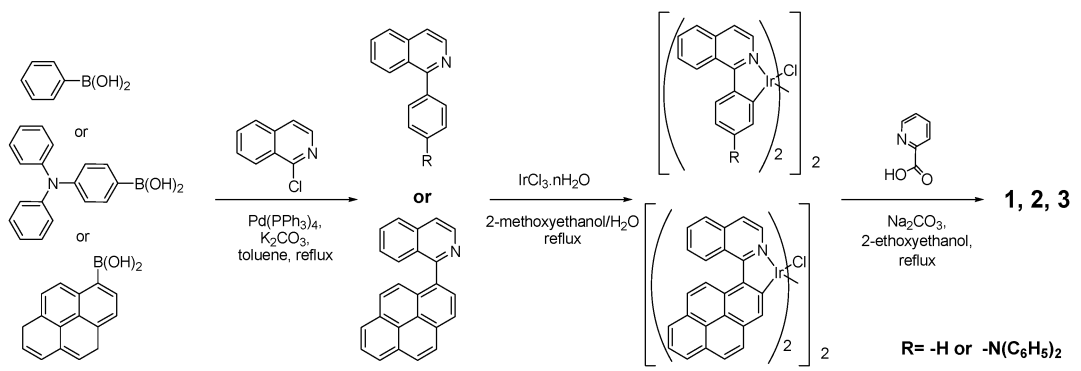

Scheme 2 Synthesis of Ir complexes.

washed with hexane and ethyl ether several times to obtain the crude product. Next, the crude chloro-bridged dimer (0.08 mmol), 3-isoquinolinecarboxylic acid (0.25 mmol), and sodium carbonate (1 mmol) were heated at reflux in 2-ethoxyethanol in an inert atmosphere for 4–5 h. After cooling to room temperature, the solvent was evaporated under high vacuum and the residue was dissolved in methylene chloride. The organic phase was then washed with water and dried over Na_2SO_4. Next, the solvent was evaporated to afford the crude product, which was subsequently purified by silica gel column chromatography. Elution was conducted using methylene chloride and methyl alcohol to obtain the desired products. The yields of **1**, **2**, and **3** were 61%, 65%, and 59%, respectively.

Complex 1. ^{1}H NMR (300 MHz, $CDCl_3$): δ (ppm) 9.00–8.95 (m, 2H), 8.76 (d, 6 Hz, 1H), 8.36 (d, 6 Hz, 1H), 8.28 (d, 6 Hz, 1H), 8.19 (d, 6 Hz, 1H), 7.95 (m, 3H), 7.77–7.71 (m, 4H), 7.62 (d, 6 Hz, 1H), 7.50 (d, 6 Hz, 1H), 7.42 (d, 6 Hz, 1H), 7.33–7.26 (m, 2H), 7.03 (t, 6 Hz, 1H), 6.95 (t, 9 Hz, 1H), 6.80 (t, 6 Hz, 1H), 6.72 (t, 9 Hz, 1H), 6.54 (d, 6 Hz, 1H), 6.24 (d, 9 Hz, 1H). ^{13}C NMR (125 MHz, $CDCl_3$): δ (ppm) 182.17, 179.50, 173.26, 153.42, 150.18, 150.10, 149.24, 148.91, 148.54, 141.45, 140.97, 138.13, 135.03, 134.24, 132.04, 131.44, 131.39, 131.02, 128.60, 128.13, 128.09, 127.26, 126.53, 126.17, 125.94, 125.16, 123.30, 122.44, 122.34, 121.70, 121.42, 118.06. HRMS (FAB) m/z: calcd. for $[C_{60}H_{42}IrN_5O_2+H]^+$ 723.1500. Found $[M+H]^+$: 723.1512.

Complex 2. ^{1}H NMR (300 MHz, DMSO-d_6): δ (ppm) 8.76 (d, 6 Hz, 2H), 8.14–8.03 (m, 5H), 8.36–8.15 (m, 2H), 7.87 (d, 6 Hz, 2H), 7.76–7.65 (m, 6H), 7.32 (d, 6 Hz, 1H), 7.13 (d, 6 Hz, 1H), 7.09–7.00 (m, 9H), 6.87 (dd, 18 Hz, 6 Hz, 13H), 6.55 (d, 9 Hz, 1H), 6.48 (d, 9 Hz, 1H), 5.81 (s, 1H), 5.57 (s, 1H). ^{13}C NMR (125 MHz, DMSO-d_6): δ (ppm) 173.17, 169.19, 167.97, 167.41, 154.08, 152.98, 152.34, 150.27, 148.83, 148.53, 148.43, 147.77, 146.87, 146.82, 146.72, 144.01, 140.73, 140.08, 138.71, 138.52, 138.43, 137.52, 136.97, 136.83, 130.82, 130.61, 130.45, 130.34, 130.00, 129.93, 129.03, 128.85, 128.75, 128.30, 128.08, 127.72, 127.46, 127.42, 127.34, 127.15, 127.00, 126.89, 126.54, 126.17, 126.04, 125.93, 125.62, 125.58, 123.92, 123.85, 123.55, 123.42, 122.48, 122.33, 119.17, 118.95, 118.29, 113.46, 113.23, 112.89. HRMS (FAB) m/z: calcd. for $[C_{60}H_{42}IrN_5O_2+H]^+$ 1057.2973. Found $[M+H]^+$: 1057.2985.

Complex 3. ^{1}H NMR (300 MHz, DMSO-d_6): δ (ppm) 8.82 (d, 6 Hz, 1H), 8.65 (d, 6 Hz, 1H), 8.38–7.69 (m, 21H), 7.38 (d, 6 Hz, 2H), 7.04–6.87 (m, 3H), 6.26 (d, 9 Hz, 1H), 6.03 (d, 6 Hz, 1H). ^{13}C NMR (125 MHz, DMSO-d_6): δ (ppm) 172.04, 171.92, 170.33, 170.00, 169.82, 169.79, 151.60, 151.31, 151.14, 149.06, 148.35, 140.78, 140.06, 139.47, 139.08, 138.92, 138.71, 137.91, 136.87, 136.69, 136.65, 132.03, 131.97, 129.74, 129.63, 129.60, 129.32, 129.20, 129.12, 129.08, 129.04, 128.97, 128.87, 128.78, 127.68, 127.51, 127.24, 127.11, 126.37, 126.32, 126.28, 126.17, 126.06, 125.96, 125.81, 125.72, 125.21, 126.06, 124.91, 124.37, 124.22, 122.03, 121.68, 121.24, 120.95, 120.87. HRMS (FAB) m/z: calcd. for $[C_{56}H_{32}IrN_3O_2+H]^+$ 971.2128. Found $[M+H]^+$: 971.2123.

Fabrication of organic photovoltaic cells

Fabrication of an organic solar cell device by spin coating: PEDOT:PSS (Baytron VP Al 4083) was spin coated for 30 s at 4000 rpm and then baked for 30 min at 140 °C. This layer was about 50 nm thick. Next, a 10 nm-thick copper phthalocyanine (CuPc) layer was thermally deposited onto the PEDOT:PSS layer. An Ir complex and PCBM were then blended in dichlorobenzene and spin-coated onto the CuPc layer in a nitrogen atmosphere. The active layer was heated on a hot plate for 30 min at 110 °C. Measurement of the thickness of the active layer using a KLA-TENCOR Alpha-step 500 profiler revealed that it was approximately 55 nm. In this procedure, CuPc was not significantly influenced by dissolution in dichlorobenzene during spin coating, as confirmed by fabrication of the devices using the thermal evaporation method. Both C_{60} and BCP were systematically deposited onto the active layer before aluminium evaporation.

Fabrication of the organic solar cell device by vacuum deposition: heterojunction solar cell A: PEDOT:PSS (Baytron VP Al 4083) was spin coated onto pre-cleaned ITO for 30 s at 4000 rpm by UV-ozone treatment and then baked for 30 min at 140 °C. The thickness of this layer was approximately 50 nm. A 10 nm-thick CuPc layer was then thermally deposited onto the PEDOT:PSS layer, after which a 20 nm-thick Ir complex was deposited and a 40 nm-thick layer of C_{60} was thermally deposited. Finally, C_{60} and BCP were systematically deposited onto the active layer before aluminium evaporation.

BHJCs B and C: after thermal deposition of CuPc onto the PEDOT:PSS layer, thermal co-deposition of **2** and C_{60} (1 : 4 ratio) was conducted. The deposition rate was controlled using quartz crystal oscillators. To control the doping ratio using one thickness monitor, the Ir complex was evaporated until the evaporation ratio became constant. The C_{60} shutter was then opened, after which the sample was heated until the thickness monitor indicated the desired doping ratio. The Ir complex shutter was simultaneously opened during the heating process. When the desired doping ratio was reached, the main shutter was opened to deposit the Ir complex and C_{60}.

Electron-only OLEDs fabrication

PEDOT:PSS (Baytron VP Al 4083) was spin-coated onto a patterned ITO glass substrate that had been pre-cleaned by UV-ozone treatment. The active layer was fabricated by spin-coating a solution of the Ir complex (10 wt%) and 4,4′-bis(9-carbazolyl)-2,2′-biphenyl (CBP) in dichlorobenzene in a nitrogen atmosphere. The other organic layers were fabricated onto the emitting layer by high-vacuum (10^{-7} Torr) thermal evaporation. A 30 nm-thick layer of 4-biphenyloxolato aluminium(III)bis(2-methyl-8-quinolinato)4-phenylphenolate (BAlq), which acted as a hole-blocking layer (HBL) and an electron-transporting layer, was deposited on the emitting layer. Subsequently, LiF, an electron injection layer (1 nm), was deposited by high-vacuum (10^{-7} Torr) thermal evaporation. Finally, the metal mask was changed and a 100 nm-thick aluminium layer was deposited onto the EIL. EL spectra were obtained using a PR 650 spectroradiometer. A source meter (Keithly 2400) connected to a computer was used to operate the device.

Results and discussion

Photophysical and electrochemical properties

As shown in Fig. 1, all Ir complexes yielded similar absorption spectra at low wavelengths owing to the π → π* transition (250–350 nm) in the main C^N ligand. However, at the wavelength at which singlet and triplet MLCT transitions occur (>400 nm),[17] the characteristics of the absorption spectrum differed from those of the main ligand present in the complex. Specifically, the presence of a triphenylamine unit in **2** produced an increase in the molar extinction coefficient (>30 000 M^{-1} cm^{-1}) in the MLCT transition range of 400–450 nm, and this molar extinction coefficient was higher than that observed for **1** (7000 M^{-1} cm^{-1}). Extension of conjugation by the addition of a pyrene unit in **3** caused the onset of the MLCT to be red-shifted, although the π → π* transitions were unaffected. Complex **3** had the highest molar extinction coefficient (>40 000 M^{-1} cm^{-1}) in the 400–450 nm region. The photoluminescence (PL) spectra of the complexes are also shown in Fig. 1. The emission spectrum of **2** (λ_{max} = 621 nm) was red-shifted with respect to that of **1** (λ_{max} = 600 nm). The emission peak of **3** was not observed because of its very low intensity; however, the λ_{max} value for the electroluminescence spectrum of OLEDs fabricated using **3** appeared to be far red-shifted (λ_{max} = 736 nm). For investigating the photo-induced charge transfer process from the donor to the acceptor, we fabricated a blending film of Ir complex : PCBM = 1 : 1. Ir complexes were used as the electron donor material, and PCBM as the electron acceptor material. As shown in Fig. S1 (ESI†), the PL of the donor was significantly quenched by PCBM. This suggested that an intermolecular photoinduced charge transfer process from the Ir complex to PCBM occurred.

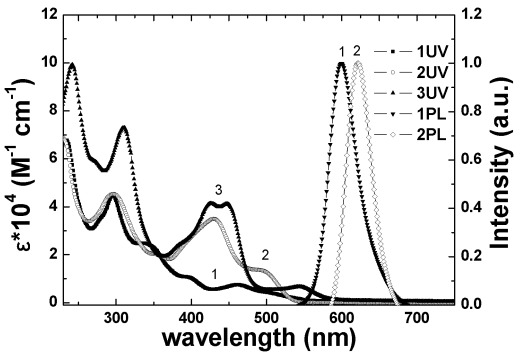

Fig. 1 Optical absorption spectra and PL spectra of Ir complexes (0.02 mM CH_2Cl_2 solution at 298 K).

The electrochemical properties of the Ir complexes were studied by cyclic voltammetry (CV). The energy levels of the highest occupied molecular orbital (HOMO) of the Ir complexes were calculated from the oxidation potentials, and the energy levels of the lowest unoccupied molecular orbital (LUMO) were obtained from the HOMO and $E_{opt,g}$ values. As shown in Table 1 and Fig. S2 (ESI†), the HOMO level was similar in complexes **1** and **2**, and the LUMO energy of **2** (−3.13 eV) was more stable than that of **1** (−3.02 eV). The HOMO and LUMO energy levels (−5.37 eV and −3.30 eV, respectively) in **3** were more stable than those in **1**. Based on these photophysical and electrochemical studies, the complexes can be arranged in the increasing order of their energy band gaps as follows: **1** > **2** > **3**.

Photovoltaic performances—spin coating method

For systematic investigation of the effect of the main ligand of the Ir complexes on the photovoltaic performance, a series of BHJCs with a multilayer structure were fabricated using a wide range of D/A blending ratios. The cell representation is as follows: ITO/PEDOT:PSS (50 nm)/CuPc (10 nm)/active layer (Ir complex was blended with PCBM before spin coating, 55 nm)/C_{60} (10 nm)/BCP (10 nm)/Al (100 nm). The cell structure was very similar to the conventional bilayer structure, except for the active layer.[5a,b] The devices were tested under AM 1.5 illumination (100 mW cm^{-2}). The current–density (*I*–*V*) characteristics are shown in Fig. 2, and the overall photovoltaic performances are summarized in Table 1.

The PCE of the devices fabricated using Ir complexes **1–3** was best when the D : A ratio was 1 : 4. A higher PCE was achieved when using **2** (0.50%) than when using **1** (0.45%). This is because the current density (J_{sc}) of **2** (2.65 mA cm^{-2}) was greater than that of **1** (2.32 mA cm^{-2}), which was due to the increased hole mobility in **2**. The presence of a triphenylamine group in **2** resulted in a slight decrease in the open-circuit voltage (V_{oc}) from 0.46 V to 0.44 V because of a slight increase in the HOMO energy of **2**. In contrast, the photovoltaic performance of **3** unexpectedly decreased to 0.34%, even though it had the highest light harvesting ability among all three complexes. The fill factor (FF) of **3** was 0.34, which was considerably lower than that of **1** (FF = 0.42) and **2** (FF = 0.43). We tentatively assumed that these results were related to the poor hole-transport capability of **3**. We attempted to confirm this assumption by fabricating electron-only OLED devices without a hole-transport layer.

Study of electron-only OLED devices

To analyze the hole-transporting capability of complexes **1–3**, we designed electron-only OLEDs (Fig. 3; Fig. S3 and S4, ESI†).

Table 1 Summary of the electrochemical and photophysical data and device performance obtained for Ir complexes **1–3**

Complex	Abs[a] (ε × 10^4 cm^{-1} mol^{-1})	E_{ox}/V *vs.* (Fc/Fc$^+$)	E_{red}/V *vs.* (Fc/Fc$^+$)	$E_{opt.g}$[b]/V	HOMO[c]/eV	LUMO[d]/eV	J_{sc}/mA cm^{-2}	V_{oc}/V	FF	PCE[e] (%)
1	296 (0.4), 341 (2.4), 400 (1.0), 460 (0.7)	0.47	−2.17	2.25	−5.27	−3.02	2.32	0.46	0.42	0.45
2	297 (0.4), 430 (3.5), 493 (1.3)	0.44	−2.20	2.11	−5.24	−3.13	2.65	0.44	0.43	0.50
3	311 (7.3), 426 (4.1), 448 (4.1), 545 (0.7)	0.57	−1.85	2.07	−5.37	−3.30	2.17	0.45	0.34	0.34

[a] 0.02 mM CH_2Cl_2 solution at 298 K. [b] Obtained at the onset of UV absorption. [c] HOMO = −(E_{ox} + 4.8 eV). [d] LUMO = HOMO + $E_{opt.g}$. [e] Device structure: ITO/PEDOT:PSS (50 nm)/CuPc (10 nm)/Ir complex + PCBM (1 : 4) (55 nm)/C_{60} (10 nm)/BCP (10 nm)/Al (100 nm).

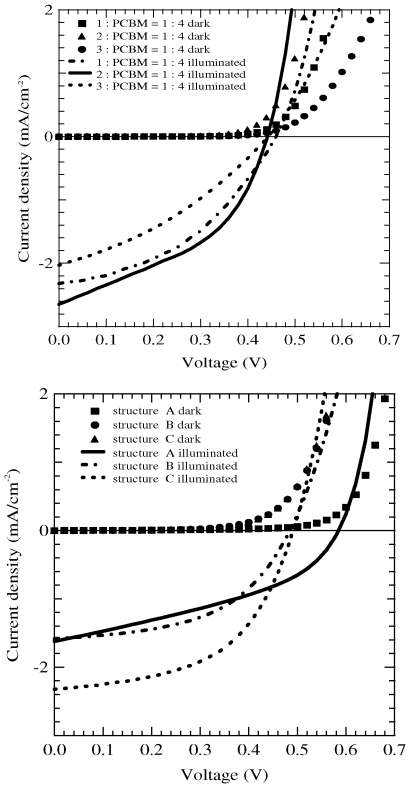

Fig. 2 *I–V* curves of Ir complex/PCBM blending systems (top) and complex **2**/C_{60} vacuum-deposition systems (bottom).

Using these devices, we investigated the relative hole mobility of the Ir complexes. The HOMO energy levels of each Ir complex affected the hole injection; however, the difference in the HOMO energies of the Ir complexes (complex **1**, −5.27 eV; complex **2**, −5.24 eV; complex **3**, −5.37 eV) was less than 0.1 eV.

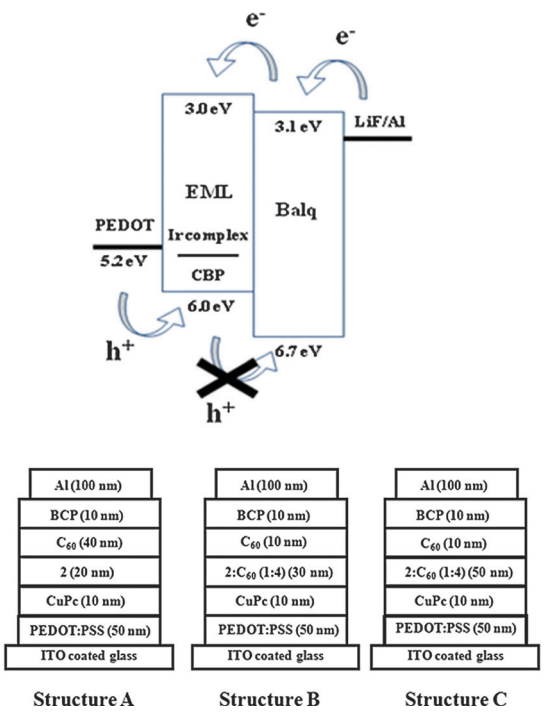

Fig. 3 Energy level diagram of an electron-only device (top) and structure of photovoltaic devices A, B, and C (bottom).

Table 2 Electron-only device performance

Complex[a]	$V_{turn-on}$/V	PE/lm W^{-1}	CE/cd A^{-1}	Emission peaks/nm
1	8.2	0.10	0.45	624
2	6.8	0.34	1.20	636
3	13	0.002	0.008	736

[a] Device structure: ITO/PEDOT:PSS (50 nm)/Ir complex with CBP (10 wt%)/BAlq (30 nm)/LiF (1 nm)/Al (100 nm).

Therefore, we assumed that the turn-on voltage ($V_{turn-on}$) and device efficiency were primarily influenced by the hole mobility of the Ir complex, with a lower $V_{turn-on}$ occurring in response to relatively better hole mobility. According to the data shown in Table 2, the complexes could be arranged in the increasing order of the $V_{turn-on}$ values as follows: **2** ($V_{turn-on}$ = 6.8 V) < **1** ($V_{turn-on}$ = 8.2 V) < **3** ($V_{turn-on}$ = 13 V). This order is in good agreement with that proposed on the basis of the photovoltaic performances of the complexes (**2** (PCE = 0.50%) > **1** (PCE = 0.43%) > **3** (PCE = 0.34%)). These results demonstrate that **2** had the relatively fastest hole mobility among the synthesized complexes. Further, the electron-only OLED fabricated using **2** was also found to have better current efficiency (CE) (1.20 cd A^{-1}), power efficiency (PE) (0.34 lm W^{-1}), and luminance (494 cd m^{-2}) than the OLED fabricated using **1**. In contrast, the lowest OLED performance of **3** was caused by its poor hole mobility. These results demonstrate that the triphenylamine unit in **2** plays a crucial role in enhancing the performance of the organic solar cell by increasing the hole mobility. Therefore, it is important to focus on the hole-transport capability when designing dyes for organic solar cells.

Photovoltaic performances—evaporation method

Because the solar cell fabricated from **2** by spin coating delivered the best performance, this dye was used to optimize the devices fabricated by the evaporation method. The *I–V* characteristics of different photovoltaic devices under AM 1.5 illumination (100 mW cm^{-2}) are shown in Fig. 2, and the performance data are summarized in Table 3. Two types of multilayer photovoltaic devices were fabricated. Device A is a multilayer heterojunction device (bilayer structure). Devices B and C are co-deposition structures that are similar to BHJCs (see Fig. 3). Because of the reduction in the effective charge separation between **2** and the C_{60} layer, the photovoltaic performance of device A fabricated by the evaporation method (PCE = 0.38%) was poorer than that of the cells fabricated by spin coating (PCE = 0.50%).

To prevent a decrease in charge separation, devices B and C were fabricated as multilayer BHJCs in which the Ir complex

Table 3 Heterojunction photovoltaic device performance

Device structure	D/A ratio	J_{sc}/mA cm^{-2}	V_{oc}/V	FF	PCE[a] (%)
A	1 : 0	1.62	0.58	0.40	0.38
B	1 : 4	1.55	0.49	0.53	0.40
C	1 : 4	2.32	0.49	0.53	0.60

[a] Device structure: see Fig. 3.

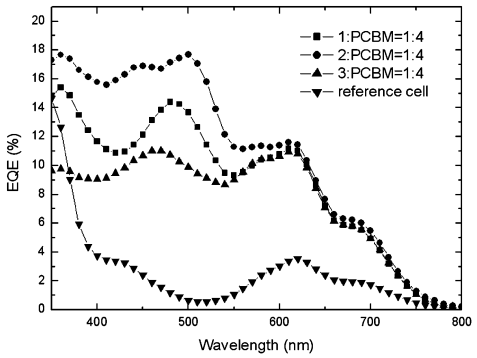

Fig. 4 The IPCE spectra with an Ir/PCBM blending layer and without a blending layer (reference cell structure: ITO/PEDOT:PSS (50 nm)/CuPc (10 nm)/C_{60} (10 nm)/BCP (10 nm)/Al (100 nm)).

and C_{60} were co-deposited in the same layer (1 : 4 ratio). The thickness of the deposited active layer was 30 nm and 50 nm in devices B and C, respectively. All other parameters corresponding to devices B and C were identical to those corresponding to device A. The lower current density of device B than device A appeared to be because of the inefficient optical depth. Conversely, when the co-deposition layer thickness was increased to 50 nm (device C), the PCE increased to 0.60% because J_{sc} of this device (2.32 mA cm^{-2}) increased considerably than those of devices A and B. The V_{oc} and FF values (0.49 V and 0.53, respectively) of device C were identical to those of device B. These results showed that by using the co-deposition method (device C), the charge separation ratio and absorption efficiency could be increased.

The EQE spectra—spin coating method

In order to address the origin of the differences in J_{sc} values, we measured the incident photon-to-current conversion efficiency (IPCE) of Ir complex/PCBM blending devices and a reference device with no blending layer, respectively. As shown in Fig. 4, Ir complexes generated photocurrent over the wavelength range from 350 to 600 nm. The complexes could be arranged in the decreasing order of the EQE values as follows: **2** > **1** > **3**. Although complex **3** exhibited the highest absorption in 380–480 nm, it showed relatively low photocurrent which could be attributed to its low hole mobility. However, there were relatively low photocurrents at >620 nm for the reference cell. The EQE was also observable in the near infrared region (over >620 nm), which resulted from the contribution of CuPc. Thus, these results supported that Ir complexes with a thin CuPc layer could be used as a panchromatic donor in the range of 400–750 nm in organic photovoltaic cells.

Conclusions

We investigated the photovoltaic performance of Ir complexes (**1–3**) with different main ligands. We used two different methods, spin coating and evaporation, for deposition of the active layer. The structure of the BHJCs fabricated using **2** (C_{60} : PCBM blending ratio, 1 : 4, spin cast) with a triphenylamine moiety in the main ligand showed the best photovoltaic performance. The photovoltaic performance of **3**, which had a pyrene unit, was relatively poor, although the energy band gap in **3** was narrower than that in **1**. The photovoltaic performance of the complexes (**2** > **1** > **3**) was dependent on their hole-transporting capabilities. The relative hole mobility of the complexes was determined by comparing the turn-on voltages of the electron-only OLED devices. The turn-on voltage of the device fabricated using **2** was lowest, demonstrating that **2** had the relatively highest hole mobility. Therefore, there should be adequate focus on the hole mobility of organic dyes when designing organic solar cells.

Moreover, the photovoltaic performance of device C fabricated by the vacuum co-deposition of **2** and C_{60} in a 50 nm-thick active layer was 50% higher than that of device A (bilayer heterojunction solar cell) and device B (fabricated by the co-deposition of **2** and C_{60} with a 30 nm-thick active layer). In spite of the low EQE, OPVs of Ir complexes generated photocurrent over the wavelength range from 350 to 600 nm. These results indicate that the co-deposition method of fabricating BHJCs effectively enhances the photovoltaic performance. This study provides the first example of the use of Ir complexes as potential donor molecules in the fabrication of organic photovoltaic cells.

Acknowledgements

This work was supported by the Basic Science Research Program through a National Research Foundation of Korea (NRF) grant funded by the Ministry of Education, Science and Technology (MEST) of Korea for the Center for Next Generation Dye-sensitized Solar Cells (No. 2011-0001055). We also thank the BK21 for fellowship grants to W. L.

References

1 C. W. Tang, *Appl. Phys. Lett.*, 1986, **48**, 183.
2 (*a*) K. Schulze, C. Uhrich, R. Schüppel, K. Leo, M. Pfeiffer, E. Brier, E. Reinold and P. Bäuerle, *Adv. Mater.*, 2006, **18**, 2872; (*b*) C. Uhrich, R. Schueppel, A. Petrich, M. Pfeiffer, K. Leo, E. Brier, P. Kilickiran and P. Bäuerle, *Adv. Funct. Mater.*, 2007, **17**, 2991.
3 (*a*) P. Peumans and S. R. Forrest, *Appl. Phys. Lett.*, 2001, **79**, 126; (*b*) M. Y. Chan, S. L. Lai, M. K. Fung, C. S. Lee and S. T. Lee, *Appl. Phys. Lett.*, 2007, **90**, 023504.
4 B. P. Rand, J. Xue, F. Yang and S. R. Forrest, *Appl. Phys. Lett.*, 2005, **87**, 233508.
5 (*a*) H. L. Wong, S. M. Lam, K. W. Cheng, K. Y. K. Man, W. K. Chan, C. Y. Kwong and A. B. Djurišić, *Appl. Phys. Lett.*, 2004, **84**, 2557; (*b*) H. L. Wong, C. S. K. Mak, W. K. Chan and A. B. Djurišić, *Appl. Phys. Lett.*, 2007, **90**, 081107; (*c*) Y. Shao and Y. Yang, *Adv. Mater.*, 2005, **17**, 2841; (*d*) F. Guo, Y.-G. Kim, J. R. Reynolds and K. S. Schanze, *Chem. Commun.*, 2006, 1887.
6 J. Roncali, *Chem. Soc. Rev.*, 2005, **34**, 483.
7 G. Yu, J. Gao, J. C. Hummelen, F. Wudi and A. J. Heeger, *Science*, 1995, **270**, 1789.
8 C. J. Brabec, A. Cravino, D. Meissner, N. S. Sariciftci, T. Fromherz, M. T. Rispens, L. Sanchez and J. C. Hummelen, *Adv. Funct. Mater.*, 2001, **11**, 374.
9 B. C. Thompson and J. M. J. Fréchet, *Angew. Chem., Int. Ed.*, 2008, **47**, 58.
10 Y. Y. Liang, Z. Xu, J. B. Xia, S. T. Tsai, Y. Wu, G. Li, C. Ray and L. P. Yu, *Adv. Mater.*, 2010, **22**, E135.
11 (*a*) Z. Xu, Z. Wu and B. Hu, *Appl. Phys. Lett.*, 2006, **89**, 131116; (*b*) C. M. Yang, C. H. Wu, H. H. Liao, K. Y. Lai, H. P. Cheng, S. F. Horng, H. F. Meng and J. T. Shy, *Appl. Phys. Lett.*, 2007, **90**, 133509.
12 (*a*) C. Adachi, M. A. Baldo, M. E. Thompson and S. R. J. Forrest, *J. Appl. Phys.*, 2001, **90**, 5048; (*b*) S. Lammansky, P. Diurovich, D. Murphy, F. Adbel-Razzaq, H. E. Lee, C. Adachi,

P. E. Burrows, S. R. Forrest and M. E. Thompson, *J. Am. Chem. Soc.*, 2001, **123**, 4304.
13 (*a*) M. Stolka, J. F. Yanus and D. M. Pai, *J. Phys. Chem.*, 1984, **88**, 4707; (*b*) Y. Shirota, *J. Mater. Chem.*, 2000, **10**, 1; (*c*) Y. Shirota, *J. Mater. Chem.*, 2005, **15**, 75.
14 A. Cravino, S. Roquet, O. Alévêque, P. Leriche, P. Frère and J. Roncali, *Chem. Mater.*, 2006, **18**, 2584.
15 (*a*) G. Zhou, W. Y. Wong, B. Yao, Z. Xie and L. Wang, *Angew. Chem., Int. Ed.*, 2007, **47**, 1149; (*b*) E. L. Williams, J. Li and G. E. Jabbour, *Appl. Phys. Lett.*, 2006, **89**, 083506.
16 M. Nonoyama, *Bull. Chem. Soc. Jpn.*, 1974, **47**, 767.
17 S. Lamansky, P. Djurovich, D. Murphy, F. A. Razzaq, R. Kwong, I. Tsyba, M. Bortz, B. Mui, R. Bau and M. E. Thompson, *Inorg. Chem.*, 2001, **40**, 1704.